Hydrodynamic functionality of the lorica in choanoflagellates

Asadzadeh, Seyed Saeed; Nielsen, Lasse Tor; Andersen, Anders; Dölger, Julia; Kiørboe, Thomas; Larsen, Poul S.; Walther, Jens H.

Published in:
Journal of the Royal Society. Interface

Link to article, DOI:
10.1098/rsif.2018.0478

Publication date:
2019

Document Version
Peer reviewed version

Hydrodynamic functionality of the lorica in choanoflagellates

Seyed Saeed Asadzadeh,[1] Lasse Tor Nielsen,[2] Anders Andersen,[3] Julia Dölger,[3] Thomas Kiørboe,[2] Poul S. Larsen,[1] and Jens H. Walther[1,4,a)]

[1)] *Department of Mechanical Engineering, Technical University of Denmark, DK-2800 Kgs. Lyngby, Denmark*

[2)] *National Institute of Aquatic Resources and Centre for Ocean Life, Technical University of Denmark, DK-2800 Kgs. Lyngby, Denmark*

[3)] *Department of Physics and Centre for Ocean Life, Technical University of Denmark, DK-2800 Kgs. Lyngby, Denmark*

[4)] *Computational Science and Engineering Laboratory, ETH, Zürich, Switzerland*

Choanoflagellates are unicellular eukaryotes that are ubiquitous in aquatic habitats. They have a single flagellum that creates a flow toward a collar filter composed of filter strands that extend from the cell. In one common group, the loricate choanoflagellates, the cell is suspended in an elaborate basket-like structure, the lorica, the function of which remains unknown. Here, we use Computational Fluid Dynamics to explore the possible hydrodynamic function of the lorica. We use the choanoflagellate *Diaphaoneca grandis* as a model organism. It has been hypothesized that the function of the lorica is to prevent refiltration (flow recirculation) and to increase the drag and, hence, increase the feeding rate and reduce the swimming speed. We find no support for these hypotheses. On the contrary, motile prey are encountered at a much lower rate by the loricate organism. The presence of the lorica does not affect the average swimming speed, but it suppresses the lateral motion and rotation of the cell. Without the lorica, the cell jiggles from side to side while swimming. The unsteady flow generated by the beating flagellum causes reversed flow through the collar filter that may wash away captured prey while it is being transported to the cell body for engulfment. The lorica substantially decreases such flow, hence it potentially increases the capture efficiency. This may be the main adaptive value of the lorica.

Keywords: Choanoflagellates, Lorica, Low Reynolds number flow, CFD, Microswimmers, Filter feeders

I. INTRODUCTION

Choanoflagellates are filter feeders and an important component of microbial foodwebs [1–3]. They share ancestry with animals and have remarkably common characteristics with the choanocytes of sponges [4]. During the past century, choanoflagellates have been subject to numerous studies with the goal of understanding the evolution of multicellularity in animals [5, 6]. Like other microswimmers, choanoflagellates live in a low Reynolds number world that is dominated by friction and very different from the inertia-dominated world of macroswimmers [7, 8]. This is important to these purely heterotrophic organisms that rely exclusively on prey captured from a very dilute suspension, requiring them to daily clear a volume of water corresponding to one million times their own body volume [9].

Choanoflagellates are equipped with a single flagellum that creates a flow toward the collar filter where bacteria-sized prey are retained on the microvilli tentacles. Some choanoflagellates (over 150 species) construct a very ornate extra-cellular basket-like structure, known as lorica [3] (Figure 1). We shall focus on the loricate choanoflagellate *Diaphanoeca grandis* that has a flagellum beating in a plane and a collar filter consisting of approximately 50 microvilli. The lorica of *D. grandis* contains 12 longitudinal and 4 transverse costae (ribs) [3] (Figure 1B). The upper part of the lorica is covered by an organic investment composed of numerous filaments (veil) woven tightly. As the flagellum beats, water enters the lorica chamber from the large spacings between the ribs in the lower part. The water is transported toward the equator and then passes through the collar filter and finally exits from the chimney. Nielsen et al. [6] demonstrated that the observed high flow rate through the collar filter of *D. grandis* can be explained by the inclusion of a flagellar vane, a structure that has been reported in closely related organisms [4, 10–13], but has not so far been observed in *D. grandis*. In the choanocytes of the leucon sponge, Asadzadeh et al. [14] demonstrated that the presence of the vane together with its interaction with the fine-meshed collar are indispensable for providing sufficiently high pressure to drive the flow through the sponge canal system [15–17].

The presence of the lorica has puzzled scientists for almost a century, and despite extensive research on the morphology, construction, and assembly of the lorica, there are only few and limited studies on its functionality [3]. Proposed functionalities are based on pure conjecture by analyzing morphological and ecological information [3]. Thus far three functions of the lorica have been proposed: First, the lorica functions as a drag-anchor that counteracts propulsion such that the force generated by the flagellum is rather spend on forcing water through the collar filter [18]. Second, the presence of the fine-meshed veil on the lorica acts in a hydrodynamic sense by funneling the inflow through the lorica and increases the water flow [18]. Third, the silicified lor-

[a)] Electronic mail: jhw@mek.dtu.dk

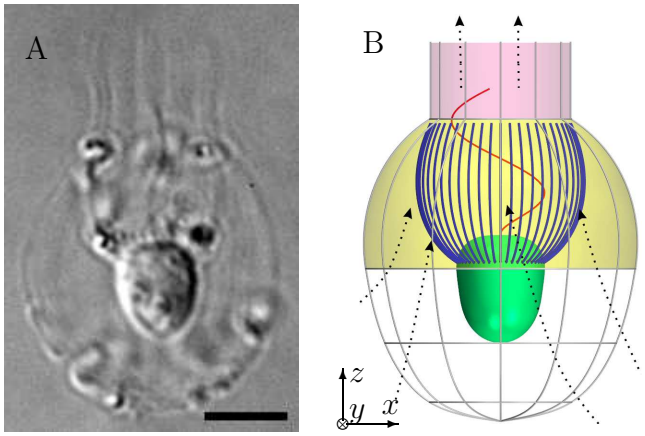

FIG. 1: Morphology of *Diaphanoeca grandis*. A) Microscopic image (scale bar: 5 μm). B) Model morphology with collar filter composed of 50 microvilli (blue), cell (green), flagellum (red), and lorica containing 12 longitudinal and 4 transvesre ribs (grey) with a fine network of filaments (the veil) on the lorica dome (yellow) and chimney (pink). The arrows indicate the direction of the flow.

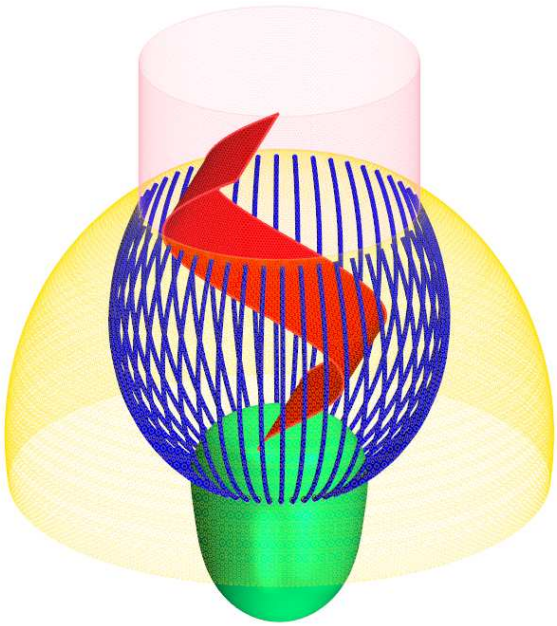

FIG. 2: CFD model morphology of *Diaphanoeca grandis* with a 5-μm wide flagellar vane (red), the microvilli (blue), and the cell (green) which are all subject to no-slip boundary conditions, and the lorica dome (yellow) and the chimney (pink) treated as porous baffle with an adjustable porosity. The ribs in the lower part of the lorica are neglected in the CFD model.

ica likely reduces the sinking velocity, especially in those species that possess spines [3], analogous to the function of spines in many diatom species [19].

Although the above suggestions seem plausible, they lack evidence and remain speculative. To examine the actual effect of the lorica, one direct approach is to study a loricate species with and without its lorica. However, as pointed out by Pettitt et al. [20] this is not a feasible experiment. Here we choose an alternative approach and use computational fluid dynamics (CFD) to study the flow around a single but representative model organism (*D. grandis*) with and without its lorica to elucidate the hydrodynamic functions of the lorica and test the validity of the proposed functionalities. Additionally, we experimentally measured the forward swimming speed of freely swimming individuals of *D. grandis*, and we used the results to validate our CFD simulations.

We first investigate the permeability of the veil on the lorica in a tethered *D. grandis*, and we find that it is practically impermeable to the flow. Modeling the lorica as an impermeable structure in the upper part, we then study the effect of the lorica on the cell motion and power consumption by the flagellum. We further study the flow rate, the flow recirculation, and the resulting clearance rate for the capture of motile and non-motile prey in the freely swimming choanoflagellate. In most cases the lorica has no beneficial role except in stabilizing the cell motion. However, the stabilized cell motion reduces the 'back-flow' through the filter and thus may increase the efficiency of prey retention on the collar filter.

II. MATERIAL AND METHODS

In this section we explain the numerical approach and the method employed for simulating a permeable lorica. We further explain the technique developed to simulate the freely swimming organism as well as our procedure to simulate advective and diffusive prey capture. Finally, we describe the experimental measurements of the swimming speed of *D. grandis*.

A. Computational Fluid Dynamics

We use Computational Fluid Dynamics (CFD) simulations to study the flow around *D. grandis*. The domain is discretized by polyhedral cells and a finite volume method is used to discretize and solve the governing equations on each cell by applying the commercial CFD program STAR-CCM+ (12.02.010-R8).

$A\,(\mu\mathrm{m})$	$L\,(\mu\mathrm{m})$	$f\,(\mathrm{Hz})$	$\lambda\,(\mu\mathrm{m})$	$W\,(\mu\mathrm{m})$
2.8	8.3	7.3	8.6	5

TABLE I: Characteristic parameters of the flagellum in *D. grandis* [6]. A is the amplitude, L the length on the central z-axis, f the frequency, λ the wavelength, and W the width of the flagellar vane.

1. Governing equations and power expenditure

The governing equations of an incompressible Newtonian fluid with density ρ and viscosity μ are the continuity and Navier-Stokes equations:

$$\nabla \cdot \mathbf{u} = 0 \tag{1}$$

$$\rho\left(\frac{\partial \mathbf{u}}{\partial t} + (\mathbf{u}\cdot\nabla)\mathbf{u}\right) = -\nabla p + \mu\nabla^2\mathbf{u} \tag{2}$$

where $\mathbf{u}$ and p denote flow velocity and pressure, respectively.

Figure 2 shows the CFD model of *D. grandis* with applied boundary conditions. Since the observed flow is only obtained by inclusion of a vane on the flagellum and not by a naked flagellum, we model this structure by a $5\,\mu$m-wide sheet which beats in a plane [6]. We model the lateral displacement of the flagellum during its beat with the following traveling wave form:

$$d(z,t) = A[1 - e^{-(z-z_B)/\delta}]\sin\left(k(z-z_B) - \omega t\right) \tag{3}$$

for $z \geq z_B$ where z_B is the z-coordinate of the flagellum at its base where it is connected to the cell, $\delta = 1.0\,\mu$m the characteristic length scale of the amplitude modulation, $k = 2\pi/\lambda$ the wave number, and $\omega = 2\pi f$ the angular frequency. The exponential term ensures that the velocity of the flagellum is zero at its base. Table I lists the characteristic parameters of the flagellum [6]. The details of the CFD model morphology for cell, filter and lorica are provided in the Supplementary Information (section IX). The Reynolds number is the ratio of inertial to viscous forces, and in small scale flows around flagellate cells it is much smaller than unity, ranging from 10^{-2} to 10^{-4} [21, 22]. Employing $\rho = 997\,\mathrm{kg/m^3}$ and $\mu = 0.001\,\mathrm{Pa\cdot s}$, here $\mathrm{Re} = \rho L^2 f/\mu \sim 5\times10^{-4}$. Therefore the inertial terms on the left hand side of Eq. (2) are negligible and the governing equations reduce to the Stokes equations that are time independent [8]. Hence, it suffices to solve the flow around the choanoflagellate at only some discrete positions of the periodically beating flagellum during a half period. However, here we solve the full Navier-Stokes equations including the unsteady and the nonlinear inertial terms that are both embedded in the STAR-CCM+ software. By retaining the unsteady term and using mesh morphing, which redistributes mesh vertices in response to the movement of the flagellum, the new position of the flagellum is updated during each time step. This method dramatically reduces the extra work of otherwise constructing the new geometry and repeated generation of the finite volume mesh.

The flagellar vane, the microvilli and the cell are subject to the no-slip boundary condition. The lorica in the upper part is treated as a permeable surface with an adjustable porosity to study the effect of the lorica pore size on the flow, but as an impermeable surface in the remainder of this study. The ribs in the lower part are neglected in the CFD simulations. The whole organism is inserted inside a spherical domain, and a pressure boundary condition is applied on the external boundary. The computational domain is discretized with 4.8 and 2.3 million computational cells for loricate and non-loricate cases, respectively. In both cases the force and the flow rate are independent of the number of cells ($\sim 2\%$ variations). For the advection and diffusion problem, the mesh is further refined on and in between the microvilli and downstream of the collar, where the concentration gradients are high, resulting in 12 and 13 million computational cells for loricate and non-loricate cases, respectively. Finally, to ensure independence of the size of the domain, we solve the governing equations on three different domain sizes with diameters of $60\,\mu$m, $80\,\mu$m and $120\,\mu$m, and we find less than 1% variations in the results. Therefore we use a domain with a diameter of $60\,\mu$m.

Once the velocity field has been determined, the power (P) expended by the beating flagellum is calculated as the surface integral over the flagellum area (S_{fl}) of its local velocity (Eq. (3)) times the resultant stress vector ($\sigma\cdot\mathbf{n}$). We verify that the total power expenditure equals the volume integral over the fluid domain (V) of the viscous dissipation:

$$P = \iint_{S_{fl}} \mathbf{u}\cdot(\sigma\cdot\mathbf{n})\,\mathrm{d}S = 2\mu\iiint_V \mathbf{E}:\mathbf{E}\,\mathrm{d}V \tag{4}$$

where $\mathbf{n}$ denotes the unit normal vector on the surface S_{fl} pointing into the fluid and $\mathbf{E} = (\nabla\mathbf{u} + (\nabla\mathbf{u})^{\mathrm{T}})/2$ the fluid strain rate tensor [23]. Equation (4) is valid for both tethered and freely swimming organism.

2. Model of the lorica as a permeable structure

The veil in the upper part of the lorica is composed of $\sim 0.01\,\mu$m thick filaments with radius $a = 0.005\,\mu$m, and it has a pore size $h = 0.05$-$0.5\,\mu$m [18]. To study the effect of the porosity of the lorica on the flow around the cell, we consider the lorica as a porous baffle that the flow can pass through subject to a pressure drop. We model this structure as a square network of cylinders of spacing h. The pressure drop (Δp_p) due to fluid flow through such a network can be related to the velocity normal to the network surface (v_n) as:

$$\Delta p_p = \frac{16\pi\mu}{h\Lambda_e} v_n \tag{5}$$

where $\Lambda_e = 1 - 2\ln\tau + \tau^2/6 - \tau^4/144 + \tau^6/1080 + ...$ and $\tau = 2\sqrt{2}\pi a/h$ [24]. Equations (1) and (2) subject to Eq. (5) are solved to obtain the velocity and pressure fields.

3. Solution procedure to model free swimming

For swimming at low Reynolds numbers, the change in the momentum is negligible compared to the pressure and viscous forces. Therefore, at any instant of time, the forces ($\mathbf{F}$) and torques ($\mathbf{L}$) of the fluid (as given by viscous and pressure forces in the stress tensor) are balanced by any external forces and torques acting on the swimmer [8]:

$$\begin{pmatrix} \mathbf{F} \\ \mathbf{L} colorbar 1_2 0 \end{pmatrix}_{\text{ext}} + \begin{pmatrix} \mathbf{F} \\ \mathbf{L} \end{pmatrix}_{\text{fluid}} = \mathbf{0} \tag{6}$$

The fluid forces and torques are calculated by integrating the stress tensor over the swimmer surface:

$$\mathbf{F} = \iint_S \sigma \cdot \mathbf{n}\, \mathrm{d}S, \quad \mathbf{L} = \iint_S \mathbf{r} \times (\sigma \cdot \mathbf{n})\, \mathrm{d}S \tag{7}$$

where $\mathbf{r}$ denotes the position on the surface S.

The motion of a microswimmer is a superposition of a deformation and a rigid body motion. The rigid body forces and torques are related to the translation velocity and rotation rate through the resistive matrix $\mathbf{R}$ of the body [8]. In our case the flagellum beats in xz-plane and because of the mirror-symmetry with respect to this plane, only translation and rotation in the xz-plane are allowed. Therefore

$$\mathbf{F}_{\text{ext}} + \mathbf{F}_{\text{def}} + \mathbf{R}\mathbf{U} = \mathbf{0} \tag{8}$$

where

$$\mathbf{F}_{\text{ext}} = \begin{bmatrix} F_x \\ F_z \\ L_y \end{bmatrix}_{\text{ext}}, \quad \mathbf{F}_{\text{def}} = \begin{bmatrix} F_x \\ F_z \\ L_y \end{bmatrix}_{\text{def}}, \quad \mathbf{U} = \begin{bmatrix} U_x \\ U_z \\ \Omega_y \end{bmatrix}$$

Here F_x and F_z denote x and z-component of the force, and U_x, U_z are the x and z-component of the velocity, respectively. L_y and Ω_y are the torque and rotation rate with respect to an arbitrary point. Here, we choose the base of the flagellum $(0, 0, z_B)$ as the point about which the organism rotates. The resistive matrix $\mathbf{R}$ is a square 3×3 matrix:

$$\mathbf{R} = \begin{bmatrix} r_{11} & r_{12} & r_{13} \\ r_{21} & r_{22} & r_{23} \\ r_{31} & r_{32} & r_{33} \end{bmatrix}$$

The unknown matrix elements depend on the shape of the organism and since the flagellum is constantly changing its shape, the matrix is also time-dependent. It can be shown that $\mathbf{R}$ is always symmetric, resulting in 6 unknowns in the matrix [25]. In the absence of any external forces and torque, the organism is freely swimming and Eq. (8) reduces to:

$$\mathbf{F}_{\text{def}} + \mathbf{R}\hat{\mathbf{U}} = 0 \tag{9}$$

where

$$\hat{\mathbf{U}} = \begin{bmatrix} \hat{U}_x \\ \hat{U}_z \\ \hat{\Omega}_y \end{bmatrix}$$

represents the swimming vector. Equation (9) represents 3 equations with 12 unknowns. However, $\mathbf{U}$ in Eq. (8) is arbitrary, and 4 appropriate choices of $\mathbf{U}$ yield 9 independent equations to solve for all elements of the matrix $\mathbf{R}$ and vector $\mathbf{F}_{\text{def}}$. This is equivalent to the problem of towing the organism with some arbitrary velocity $\mathbf{U}$ and imposing the external forces and torque that equal the fluid forces and torque calculated by Eq. (7). Once these quantities are found, the swimming vector $\hat{\mathbf{U}}$ is determined by Eq. (9).

The arbitrary choices of the vector $\mathbf{U}$ in Eq. (8) are as follow:

1. $\mathbf{U} = \begin{bmatrix} 0 \\ 0 \\ 0 \end{bmatrix}$ gives $\mathbf{F}_{\text{def}}$
2. $\mathbf{U} = \begin{bmatrix} 1 \\ 0 \\ 0 \end{bmatrix}$ gives r_{11}, $r_{21} = r_{12}$ and $r_{31} = r_{31}$
3. $\mathbf{U} = \begin{bmatrix} 0 \\ 1 \\ 0 \end{bmatrix}$ gives r_{22} and $r_{32} = r_{23}$
4. $\mathbf{U} = \begin{bmatrix} 0 \\ 0 \\ 1 \end{bmatrix}$ gives r_{33}

Finally, once the swimming vector $\hat{\mathbf{U}}$ is determined, one more simulation is conducted to obtain the pressure and velocity fields, and to extract the forces on the different body parts of the choanoflagellate in the freely swimming form. The above calculations have been performed independently for 12 different positions of the flagellum during the first half of its beat period.

4. Advection and diffusion of prey

In loricate choanoflagellates the structure of the lorica is such as to guide the flow through the lorica chamber [3]. In *D. grandis* specifically, the beating flagellum sucks in the water from the lower part of the lorica through the equator and expels it out from the chimney resembling a jet [6]. This arrangement may suggest that the cell is directing the water far away from itself in order to prevent refiltration of once filtered water, a phenomenon which

the volume flow rate *per se* does not account for. To test this hypothesis, we assume that prey concentration (C) satisfies the advection-diffusion equation [26, 27]:

$$\frac{\partial c}{\partial t} + \mathbf{u} \cdot \nabla c = D \nabla^2 c \tag{10}$$

where $c = C/C_\infty$ is the dimensionless concentration field, C_∞ the concentration of the prey in the far field, and D the diffusivity of the prey due to Brownian motion and motility. The collar filter acts as a sink and consumes the prey once it reaches it, essentially leading to a vanishing value of c. To model this behaviour, we set $c = 0$ in a thin volume inside the collar filter, in close proximity of the microvilli using a source term that is active in this region [28]. We set $c = 1$ on the outer boundary where the flow enters the domain. Initially the concentration inside the collar filter volume is zero and elsewhere $c = 1$. Both the advective and the diffusive transport through the filter contribute to the clearance rate:

$$Q_{net} = -\int_{S_{filter}} (c\mathbf{u} - D\nabla c) \cdot \mathbf{n} \, \mathrm{d}S \tag{11}$$

The simulations are performed for 40 beat cycles at which time the flow is sufficiently developed and periodicity in the net clearance rate has been obtained.

B. Observed swimming speed

Diaphanoeca grandis (American Type Culture Collection no. 50111) was cultured non-axenically in the dark at 10°C, using B1 medium with a salinity of 32. Organically grown, autoclaved rice grains were added as bacterial substrate [6]. To determine the swimming speed, freely swimming *D. grandis* cells were observed using an Olympus IX-71 inverted microscope equipped with a UPLSAPO60XO/1.35 oil-immersion objective and a U-ECA magnifying lens. Image sequences were recorded at 100 frames per second and a resolution of 1024×800 pixels using a Phantom v210 high-speed camera. Observations were done in a chamber constructed from a 5 mm high polycarbonate ring (diameter ∼1 cm) mounted with non-hardening silicone between an objective slide and a coverslip.

III. RESULTS AND DISCUSSION

A. Permeability of the lorica

In this section we simulate a tethered *D. grandis* and model the lorica as a porous structure with a range of pore sizes between 0.05 and 0.5 μm. Figure 3 depicts the velocity field in the xz-plane for the two different pore sizes of 0.05 and 0.5 μm averaged over the flagellum beat cycle. A pore size of 0.05 μm practically acts as an impermeable structure (Figure 3A). However, as the porosity increases from 0.05 to 0.5 μm, the lorica becomes permeable to the flow (Figure 3B), in response to the negative pressure created below the lorica dome (Eq. (5)). Consequently, a portion of the flow reaching the collar filter passes through the lorica dome which results in less flow entering the collar filter through the equator plane. Figure 3C shows the time-averaged flow rate through the equator plane, the collar filter, and the lorica dome for a complete beat cycle. The flow through the filter is almost independent of the lorica porosity, and for all cases it is very close to the volume flow rate approximated by the pumping mechanism value of $Q_V = AW\lambda f = 879\,\mu\mathrm{m}^3/\mathrm{s}$ proposed by Nielsen et al. [6] (Eq. 5 therein). This is because the flagellum acts nearly as a positive displacement pump in a system of small overall resistance as flow shifts between paths for changing lorica porosity.

Since only the collar filter captures prey, the lorica blocks prey larger than its pore size (i.e. typical bacteria-sized prey) from reaching the filter. Thus, only flow passing the equator plane provides nutrition for the cell, and this decreases as the porosity of the veil increases. This suggests that the lorica costae either should be covered with a fine mesh, virtually impermeable to the flow, or with a very coarse mesh not to intervene in the prey capture process. An intermediate pore size allows water to pass through while intercepting bacteria-sized prey, consequently impairing the feeding process. In fact, the lorica either contains a fine veil, as compared to the filter spacing, or in some species it appears as an open structure [3]. Nevertheless, even with a medium pore size, more than 80% of the flow goes through the equator plane. Therefore, modeling the lorica as an impermeable structure in the CFD study is an acceptable approximation to the actual structure, and henceforth, employing the previously used CFD model [6], we consider the lorica as an impermeable baffle subject to the no-slip boundary condition.

B. Swimming motion and power expenditure

Loricate choanoflagellates are generally slow swimmers compared to non-loricate species [3, 18]. Figure 4 shows the velocity components and the rotation rate of our modeled freely swimming *D. grandis* with and without its lorica. The forward swimming velocity ($\hat{U}_z$) of *D. grandis* varies slightly during the half cycle with a mean value of 3.0 μm/s (Figure 4A). This is in agreement with experiments where the forward swimming velocity $U_{exp} = 2.2 \pm 1.1\,\mu$m/s was obtained as the average of 6 different individuals of *D. grandis*. The forward swimming is the dominant motion of the choanoflagellate and the lateral velocity and rotation are relatively small (Figures 4B and 4C). As a result, *D. grandis* swims smoothly forward along a rather straight line without additional motion (Movies S1 and S2). When the lorica is removed, the choanoflagellate appears to remain a slow swimmer with a mean forward swimming velocity of 3.1 μm/s very

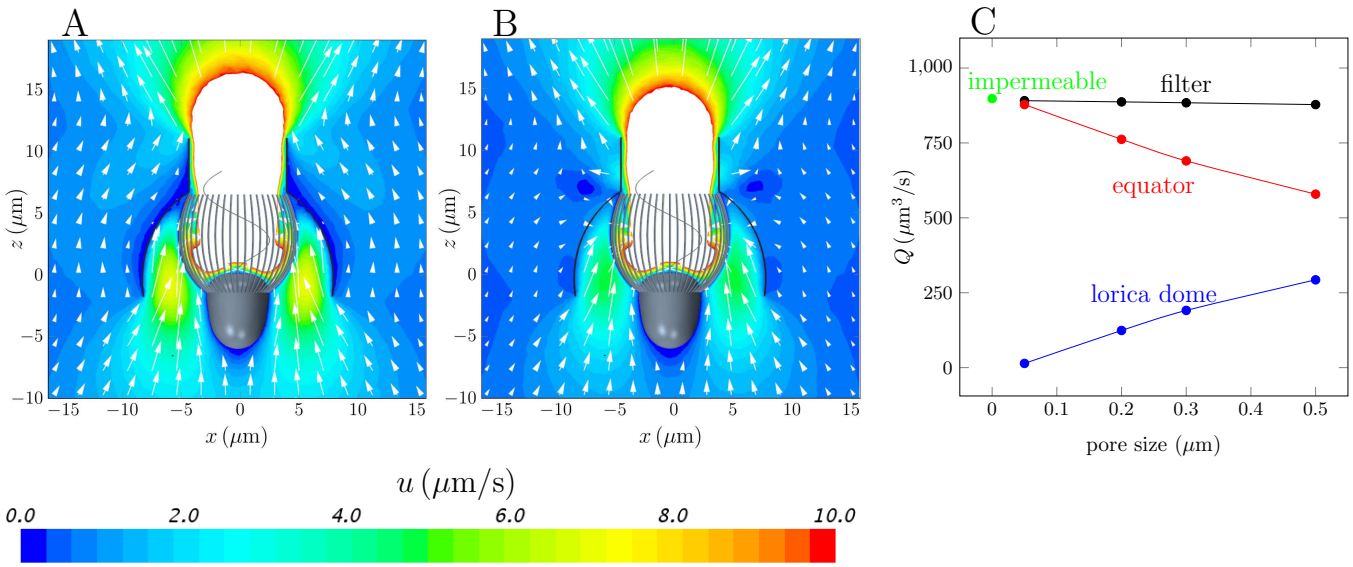

FIG. 3: Dependence of flow velocities and flow rates on the permeability of the lorica. Velocity field in the xz-plane for the lorica pore sizes of 0.05 μm (A) and 0.5 μm (B) time-averaged over the flagellum beat cycle. For clarity, the velocity magnitudes higher than 10 μm/s are omitted. (C) Mean flow rate through the filter, equator plane and lorica dome for different pore sizes of the lorica. As the pore size increases, the volume flow rate through the equator plane decreases while more flow permeates through the lorica dome which intercepts the prey particles larger than its pore size. The flow through the collar filter is independent of the lorica pore size and very close to the case of an impermeable lorica.

close to that of the loricate one. However, in this case, the lateral velocity components and rotation rate are significant and the cell wiggles from side to side as it swims forward (Movie S3). Hence, the lorica appears to stabilize the movement of the cell.

It is striking that the forward swimming velocity of *D. grandis* is almost independent of the presence of a lorica since previously it has been suggested that the lorica slows down the forward motion by imposing a significant drag that counteracts the locomotory flagellum force [18]. Table II lists the force in the swimming direction on different parts of *D. grandis* with and without its lorica in the freely swimming form, as well as in the case of externally towed, rigid body with a mean swimming velocity of 3 μm/s. In the freely swimming *D. grandis* the flagellum force nearly balances the drag on the body and filter, while the drag on the lorica is insignificant.

The reason that the large lorica does not create significant drag is that the flow is driven "internally" by the beating flagellum. The resulting flow differs markedly from the flow around the towed cell (Figure 5). In the latter, the drag force is owing to positive contributions of both the pressure and shear forces [25]. However, in an internal flow, the pressure contribution can counteract the viscous forces depending on the shape of the object and its interaction with other body parts, resulting in a smaller net drag force. This is the case for the lorica, for which the flow is internal. The time-averaged pressure field in the xz-plane reveals a low pressure region right below the lorica dome which creates a suction region pulling the lorica down (Figure 6). As a result, the pressure force acts in the opposite direction of the flow and counteracts the shear drag such that the net drag on the lorica is comparably small.

When *D. grandis* is towed (or is exposed to an external flow), the drag on the lorica plays a significant role, contributing 86 % to the total drag (Table II). However, the force on the lorica is very small in comparison with the force due to the beating flagellum of the freely swimming organism. In addition, the presence of the lorica significantly decreases the drag force on the filter and the cell by factors of 7.7 and 7.1, respectively. The lorica increases the total external drag force on the choanoflagellate by 52% (Table II).

Finally, Figure 7 shows the mechanical power consumption by the flagellum over a half cycle for *D. grandis* with and without its lorica; the average power consumption is 2.20 and 1.75 fW, respectively. To compare these values to the metabolic budget of the choanoflagellate, we use the size dependent mass-specific metabolic rate for the flagellate, $\mathrm{RR} = 173\,\mathrm{M}^{0.17}$ [29], where RR is the specific respiration rate in $\mu\mathrm{l\,O_2\,mg\,C^{-1}\,h^{-1}}$ and M the body mass of the organism in mgC. As an estimate of the carbon content, we take 10% of the organism mass, resulting in 9.2×10^{-9}mgC. To relate the respiration rate to metabolic rate, we use a standard oxycalorific value of 13.8 $\mathrm{J\,mg\,O_2^{-1}}$ [30, p. 592] which gives a value of 375 fW, two orders of magnitudes bigger than the power expen-

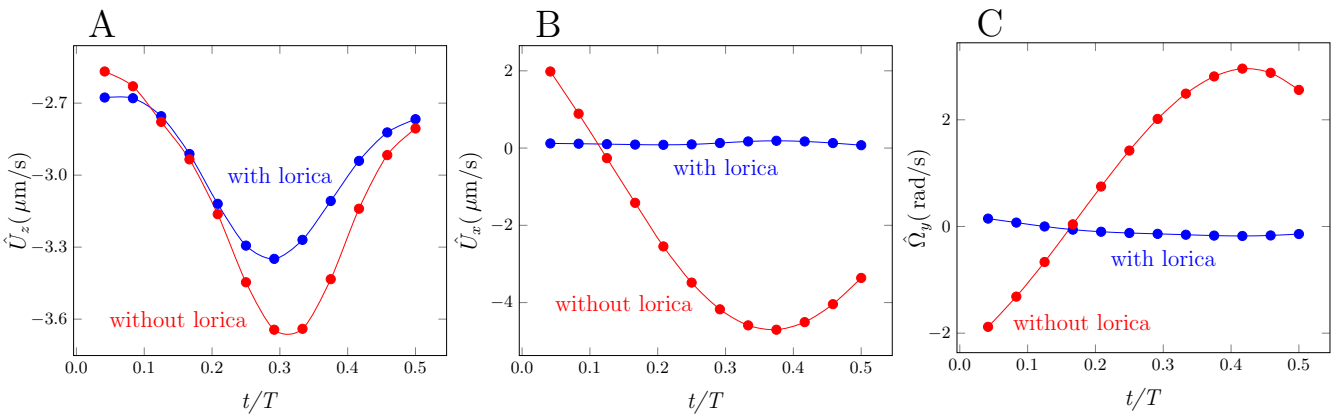

FIG. 4: Velocity components and rotation rate during one half cycle for *Diaphanoeca grandis* with and without its lorica. The presence of the lorica does not significantly alter the swimming velocity (A), but it dampens significantly the lateral velocity (B) and the rotation rate (C).

Case		Force (pN)				
		Flagellum	Cell	Filter	Lorica	Total
Freely swimming	With lorica	-12.091	4.343	7.169	0.580	0.001
	Without lorica	-8.522	3.344	5.173	-	0.004
Towed	With lorica	0.027	0.008	0.027	0.382	0.444
	Without lorica	0.027	0.057	0.208	-	0.292

TABLE II: The z-component of the force on different parts of *Diaphanoeca grandis* with and without its lorica in the freely swimming and towed choanoflagellate with velocity of $3\,\mu$m/s in the swimming direction.

diture by the flagellum. Even though the efficiency of conversion is not 100%, the relative cost of beating the flagellum is low, and therefore the additional power consumption with the lorica is insignificant.

C. Clearance rate

This section presents the effect of the lorica on the clearance rate in the freely swimming choanoflagellate. First we discuss the flow rate through the collar filter, i.e. neglecting the diffusion and depletion of the prey, and then on the net clearance rate where advection and diffusion of the prey are considered.

1. Flow rate through the collar filter

In the absence of prey diffusion, Eq. (11) gives the volume flow rate Q by setting $c = 1$ (the case $D = 0.0$ marked with asterisk in Table III). The lorica has a slight effect on the volume flow rate increasing it only by $\sim$5 %. This is consistent with the result of section III A where the flow passing through the filter is shown to be unaffected by the lorica porosity.

Another important aspect is that the slow swimming motion of *D. grandis* does not significantly increase the volume flow rate as compared to the tethered value of $Q = 898\,\mu\mathrm{m}^3/\mathrm{s}$ in the previous study [6]. This is because of a significant resistance by the cell, the filter and the lorica to the swimming, and most of the flow bypasses the collar filter (Figure 5, C and D).

2. Advection and diffusion effect

The volume flow rate does not reveal possible effects of flow recirculation and prey diffusivity on feeding. Flow recirculation, i.e. backflow from downstream of the chimney toward the upstream of the lorica, can potentially imply refiltration of already filtered water. To determine a more correct volume cleared for prey, we study the net clearance rate Q_{net} of Eq. (11) including advection and diffusion of the prey. Table III lists the net clearance rate for different values of prey diffusivity. First we consider only advection of a passive prey ($D = 0.0$), i.e. in the

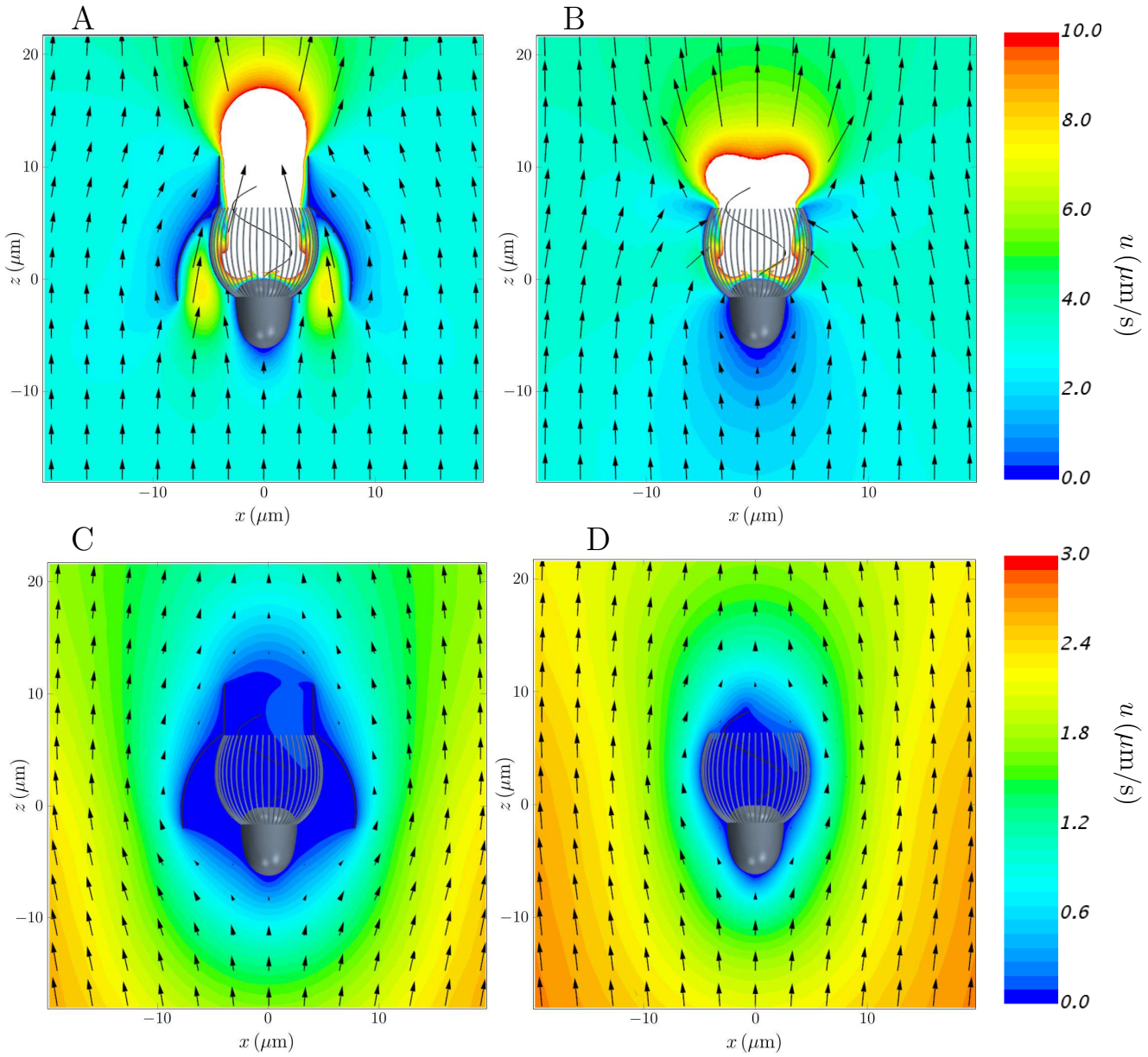

FIG. 5: Flow fields in the freely swimming and towed choanoflagellates in the frame of reference moving with the cell. A and B) Velocity field around freely swimming *Diaphanoeca grandis* with and without its lorica averaged over the flagellum beat cycle. C and D) Velocity field around the towed *D. grandis* with and without its lorica with a velocity of $3\,\mu$m/s. The flow near and through the lorica and the filter is dominated by the beating flagellum. Moreover, when towed, the presence of the lorica reduces the flow velocity over the cell and hence reducing the force on the cell and the collar filter.

limit of infinite Péclet number. This case is suitable to study the possible recirculation of the flow. Here there is only a minor difference (-5.2%) in the net clearance rate of *D. grandis* with and without its lorica. The function of the lorica is thus not to prevent recirculation.

The case $D = 0.4\,\mu\text{m}^2/\text{s}$ in Table III corresponds to the effective diffusivity due to the Brownian motion of a typical spherical prey of $0.5\,\mu$m in diameter at 16 °C. In this regime the advective transport is dominant, and the difference in the clearance rate is still small. Although the chimney in *D. grandis* directs the flow far from the choanoflagellate resembling a jet, there is still no sign of recirculation even after the lorica is removed (Figure 8A). However, as we increase the diffusivity D, i.e. smaller Péclet number, the clearance rate becomes dominated by the diffusion mechanism. At $D = 30\,\mu\text{m}^2/\text{s}$, which is the

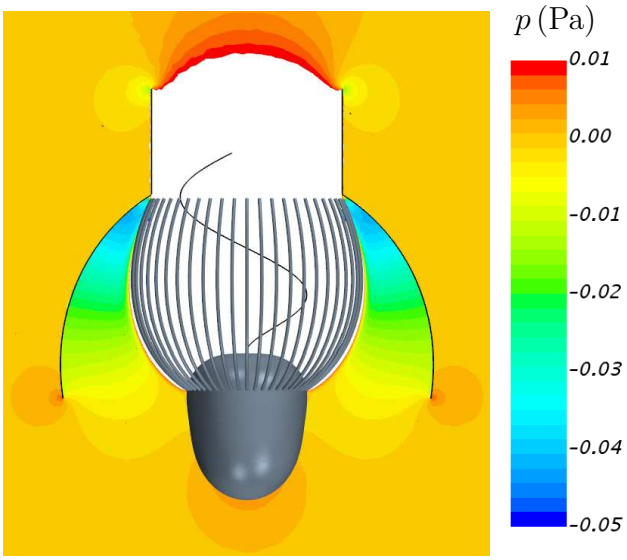

FIG. 6: The time-averaged pressure field in the xz-plane around the freely swimming *D. grandis* reveals a low pressure region right below the lorica dome which results in a pressure force in the swimming direction. For clarity, the pressure inside the filter and chimney is not shown.

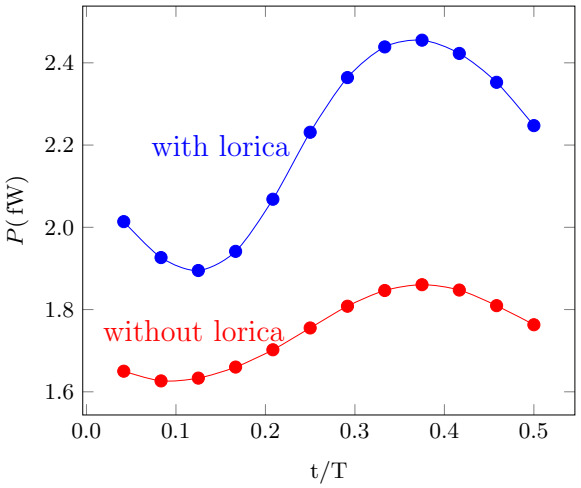

FIG. 7: Power consumption by the flagellum for *Diaphanoeca grandis* with and without its lorica. The presence of the lorica increases the average required power by $\sim$ 25%, however the power magnitudes are insignificant when compared to the metabolic rate.

effective diffusivity of a typical motile prey with swimming speed 44 μm/s and run time 0.04 s [31], the net clearance rate of the non-loricate choanoflagellate surpasses the loricate one by 67% (Table III). In a pure diffusive transport regime, the flux through a spherical sink in an infinite domain is $Q_{diff} = 4\pi D R_{sink}$ where R_{sink} is the radius of the sink [32]. Employing a mean filter radius

$D\,(\mu\text{m}^2/\text{s})$	$Q_{net}\,(\mu\text{m}^3/\text{s})$		$\Delta\,(\%)$
	with lorica	without lorica	
0.0*	902	867	-3.9
0.0	900	853	-5.2
0.4	904	860	-4.9
4.0	920	950	3.3
30.0	1290	2150	66.7

TABLE III: Mean clearance rate Q_{net} for different values of diffusivity D. Δ is percentage difference in Q_{net} with and without lorica. *corresponds to the volume flow rate Q which is obtained by setting $c = 1$ in Eq. (11).

of $R_f = 4.3\,\mu$m and a diffusivity of $D = 30\,\mu\text{m}^2/\text{s}$, for the case without the lorica we find $Q_{diff} = 1620\,\mu\text{m}^3/\text{s}$ comparable with the total clearance rate indicating the complete dominance of diffusive transport when prey motility is considered. In such a diffusion dominated regime, the lorica suppresses the prey transfer toward the filter (Figure 8B). This suggests that loricate choanoflagellates are inefficient feeders on motile bacteria.

D. Prey retention

Thus far, our results on clearance rates for different scenarios and energy expenditure reveal no significant advantage of the lorica, but rather the opposite for motile prey. However, the clearance rate estimated above assumes that all encountered prey are captured. One should also consider the efficiency of prey capture, that is the ratio of the number of prey particles captured to those encountered. Filter feeding consists of three successive steps: prey encounter, retention and handling [33]. Once the prey is in contact with the microvilli during the encounter process, the cell must retain and transfer it down to the base of the collar toward the cell where it is phagocytosed. This process may take several seconds [20], and in the choanoflagellate *Salpingoeca rosetta*, Dayel et al. [34] report that the movement of bacteria prey to the base and engulfing takes on average 12.5 s and 20 s, respectively. Given that the flagellum beat period in choanoflagellates is a fraction of a second, the prey experiences hundreds of beat cycles as it is being moved along the collar, with a potential to be lost before being engulfed. We speculate that the lorica increases the efficiency of prey capture by three mechanisms.

Firstly, without lorica, the cell and specifically the microvilli exhibit intense movements from side to side, which possibly hinders prey retention and transportation down to the base of the collar. However in the loricate cells, the lorica stabilizes the cell motion by reducing the lateral motion of the cell and microvilli which could reduce the risk of prey escape. Being thecate or part of a colony could have a similar effect where the cells attach to a substrate or stick together via filopodia and inter-

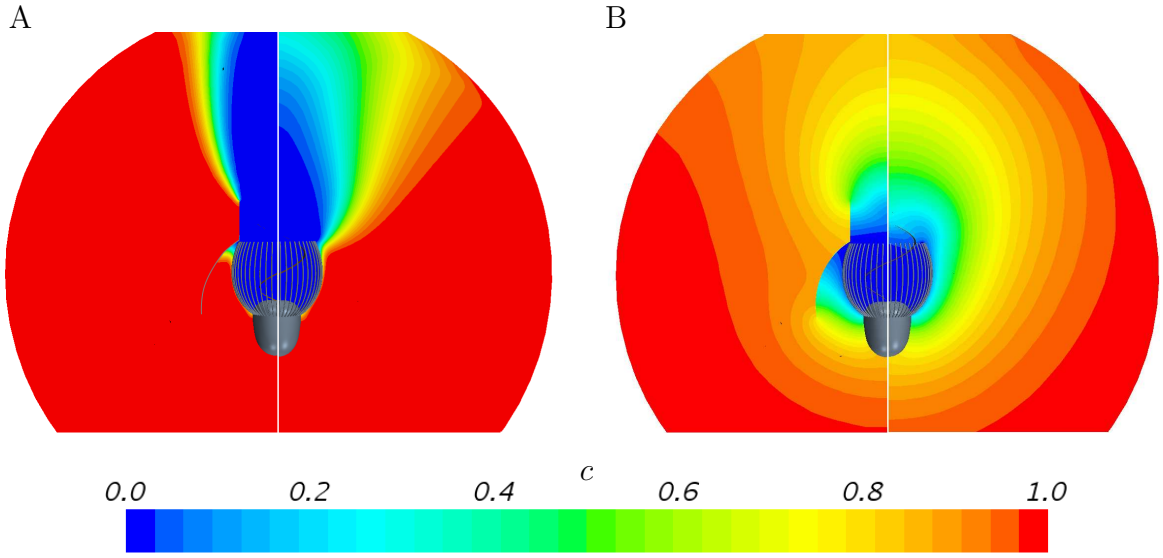

FIG. 8: Prey concentration (c) in the xz-plane around the freely swimming *Diaphanoeca grandis*. A) $D = 0.4\,\mu\text{m}^2/\text{s}$ which corresponds to the effective diffusivity of typical passive prey due to Brownian motion. B) $D = 30\,\mu\text{m}^2/\text{s}$ which corresponds to the effective diffusivity of typical motile prey. For each case, the left and right half of the plot shows the result with and without its lorica, respectively. At small diffusivity (high Pe), the advection is the dominating transport factor while at higher diffusivity (low Pe), the diffusion becomes dominant. In this case the lorica would act as an insulation to prey diffusion towards the filter, thus reducing the net clearance rate as compared to that of the non-loricate case.

cellular bridges [35–37]. Attachment or colony formation stabilizes the individual cell and the collar motion, potentially increasing the retention efficiency. This could also be the reason why the flagella beat is not synchronized in colonies [38, 39], as the lateral force and torque from neighbouring cells would stack rather than cancel out.

Secondly, while the flagellum is beating, in some areas at the distal part of the microvilli, the flow direction is outward from the collar. This phenomenon is observed in both loricate and non-loricate cells, but it is much more intense in the latter. Figure 9 depicts snapshots of the velocity field between the microvilli in the xz plane. Without lorica, the velocity in the upper part of the collar is outward and bigger in magnitude than for the loricate one. Including the lorica mitigates this effect not only by lowering the velocity magnitude, but also by slight downward deflection of the flow. This may increase the likelihood of prey retention on the collar. For the cell to retain a passive prey that encounters the outer surface of the microvilli, the adhesive force by the collar must equal or exceed the local fluid forces resisting the adhesion [33]. For a given adhesive force, the smaller the local fluid forces on the particle, the bigger the likelihood of the bacteria retention on the collar. The lorica reduces velocities on the distal part of the filter, and thus could improve prey retention. Poor particle retention and loss of bacteria from the distal part of the collar has been observed in some species of non-loricate choanoflagellates such as *Salpingoeca amphoridium* [40] and *S. rosetta* single cells and colonies [34]. Another remedy to this problem would be to have the prey capture zone mostly on the lower part of the microvilli where there is no outflow; the veil in the loricate choanoflagellate *Didymoeca costata* guides the inflow directly toward the collar base [3] where the prey is immediately captured and ingested.

Thirdly, the lorica chamber, especially in species with a veil on the inner surface of the lorica such as *D. grandis, D. costata* and *Crinolina aperta*, is similar to a trap; even if the prey escapes from the collar, the lorica veil does not allow it to go beyond reach and it is more likely for the choanoflagellate to recapture its prey.

IV. CONCLUSION

In this study, using detailed CFD simulations, we explore the hydrodynamic function of the lorica in the standard tectiform loricate choanoflagellate *Diaphanoeca grandis*. Our results provide no support for the several previous hypotheses regarding the effects of the choanoflagellate lorica. Rather, our simulations suggest that the main function of the lorica is to enhance the capture efficiency, but this happens at the cost of lower encounter rate with motile prey. We note that our study concerns mainly hydrodynamic effects of the lorica. There could well be other effects of the lorica, including e.g. protection against predators.

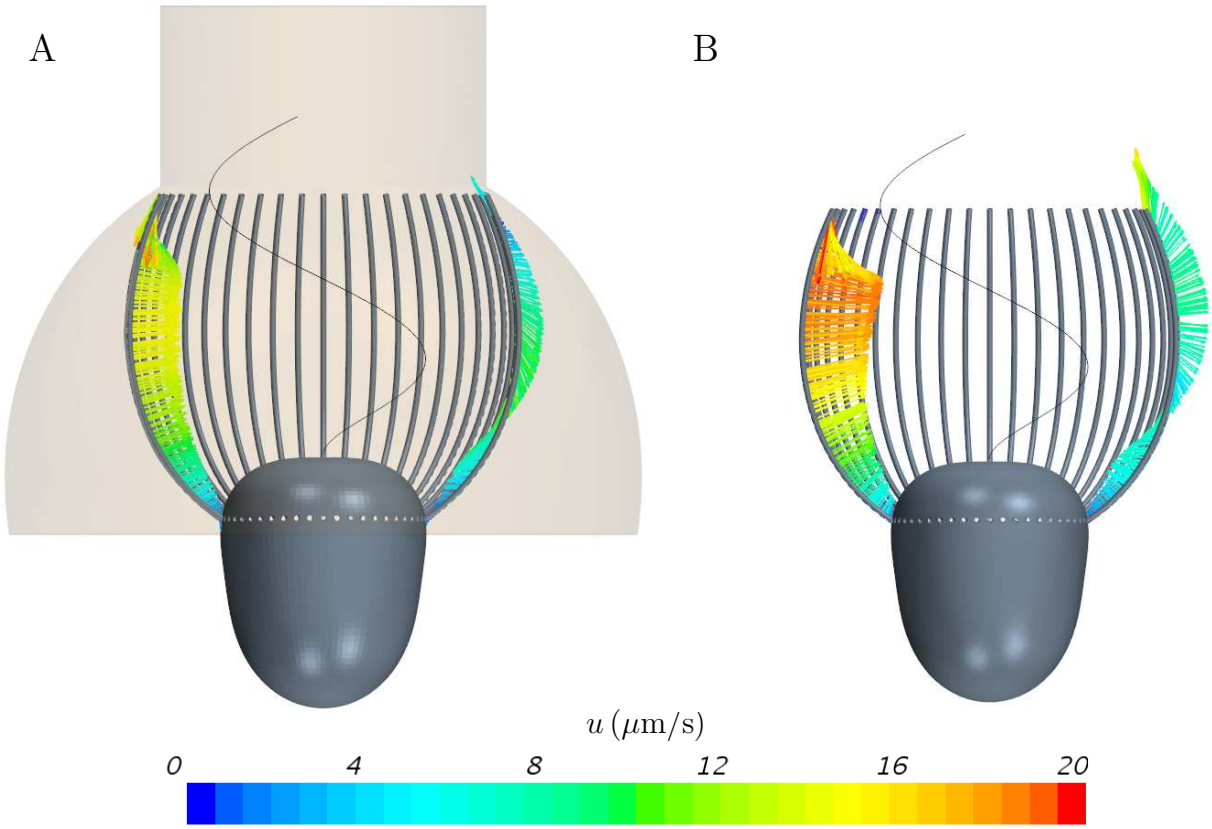

FIG. 9: Snapshot of the velocity field between the microvilli in the flagellar beat plane (xz-plane) of *Diaphanoeca grandis* with (A) and without (B) its lorica. The lorica mitigates the outward flow from the distal part of the microvilli, potentially increasing the chance of retaining the prey on the collar.

V. DATA ACCESIBILITY

All data for the model morphology and numerical modeling are described in this paper.

VI. AUTHORS' CONTRIBUTIONS

All authors designed the research and wrote the paper. SSA, AA, JD, PSL and JHW developed the model and the matematical framework for the CFD simulations. LTN and TK provided biological advice on the model and interpreting the results. LTN did the experiment. SSA performed the simulations.

VII. COMPETING INTERESTS

The authors declare no competing interests.

VIII. FUNDING

We gratefully acknowledge funding from the Villum Foundation for SSA and JHW through research grant (9278) and for AA, JD, LTN, and TK through the Centre for Ocean Life. TK, AA, and LTN were further supported by The Danish Council For Independent Research (grant 7014-00033B).

[1]Tom Fenchel. Suspended marine bacteria as a food source. In *Flows of energy and materials in marine ecosystems*, pages 301–315. Springer, 1984.

[2]Tom Fenchel. Protozoan filter feeding. *Prog. Protistol.*, 1:65–113, 1986.

[3]Barry S. C. Leadbeater. *The Choanoflagellates: Evolution, Biology and Ecology*. Cambridge University Press, Cambridge, 1 edition, 2015.

[4]Jasmine L. Mah, Karen K. Christensen-Dalsgaard, and Sally P. Leys. Choanoflagellate and choanocyte collar-flagellar systems and the assumption of homology. *Evol. & Develop.*, 16(1):25–37, 2014.

[5]Manuel Maldonado. Choanoflagellates, choanocytes, and animal multicellularity. *Invertebrate Biol.*, 123(1):1–22, 2004.

[6]Lasse Tor Nielsen, Sayed Saeed Asadzadeh, Julia Dölger, Jens H. Walther, Thomas Kiørboe, and Anders Andersen. Hydrodynamics of microbial filter feeding. *Proc. Natl. Acad. Sci. USA*, 114(35):9373–9378, 2017.

[7] E. M. Purcell. Life at low Reynolds number. *Am. J. Phys.*, 45(1):3–11, 1977.

[8] Eric Lauga and Thomas R. Powers. The hydrodynamics of swimming microorganisms. *Rep. Prog. Phys.*, 72(9):096601, 2009.

[9] Thomas Kiørboe. How zooplankton feed: mechanisms, traits and trade-offs. *Biol. Rev.*, 86(2):311–339, 2011.

[10] Ejnar Jules Fjerdingstad. The ultrastructure of choanocyte collars in *Spongilla lacustris* (l.). *Z. Zellforsch.*, 53(5):645–657, 1961.

[11] Dorte Mehl and H. M. Reiswig. The presence of flagellar vanes in choanomeres of Porifera and their possible phylogenetic implications. *J. Zoo. Sys. Evol. Res.*, 29(4):312–319, 1991.

[12] Norbert Weissenfels. The filtration apparatus for food collection in freshwater sponges (Porifera, Spongillidae). *Zoomorph.*, 112(1):51–55, 1992.

[13] Barry S. C. Leadbeater. The mystery of the flagellar vane in choanoflagellates. *Nova Hedwigia Beiheft*, 130:213, 2006.

[14] Sayed Saeed Asadzadeh, Poul S. Larsen, Hans Ulrik Riisgård, and Jens H. Walther. Hydrodynamics of the leucon sponge pump. *J. Roy. Soc. Inter*, (submitted), 2018.

[15] Poul Scheel Larsen and Hans Ulrik Riisgård. The sponge pump. *J. Theor. Biol.*, 168:53–63, 1994.

[16] S. P. Leys, G. Yahel, A. Reidenbach, V. Tunnicliffe, U. Shavit, and H. Reiswig. The sponge pump: the role of current induced flow in the design of the sponge body plan. *PLoS one*, 6(12):e27787, 2011.

[17] D. A. Ludeman, M. A. Reidenbach, and S. P. Leys. The energetic cost of filtration by demosponges and their behavioural response to ambient currents. *J. Exp. Biol.*, 220(6):995–1007, 2017.

[18] Per Andersen. Functional biology of the choanoflagellate *Diaphanoeca grandis Ellis*. *Marine Microbial Food Webs*, 3(2):35–50, 1988.

[19] A. E. Walsby and Anastasia Xypolyta. The form resistance of chitan fibres attached to the cells of Thalassiosira fluviatilis Hustedt. *British Phycological Journal*, 12(3):215–223, 1977.

[20] Michala E. Pettitt, Belinda A. A. Orme, John R. Blake, and Barry S. C. Leadbeater. The hydrodynamics of filter feeding in choanoflagellates. *Eur. J. Protist.*, 38:313–332, 2002.

[21] J. J. L. Higdon. A hydrodynamic analysis of flagellar propulsion. *J. Fluid Mech.*, 90(4):685–711, 1979.

[22] M. A. Sleigh. Mechanisms of flagellar propulsion. *Protoplasma*, 164(1-3):45–53, 1991.

[23] G. K. Batchelor. *An Introduction To Fluid Dynamics*. Cambridge University Press, 1. edition, 1967.

[24] N. R. Silvester. Some hydrodynamic aspects of filter feeding with rectangular-mesh nets. *J. Theor. Biol.*, 103(2):265–286, 1983.

[25] John Happel and Howard Brenner. *Low Reynolds number hydrodynamics*. Kluwer Academic Publishers, 2 edition, 1983.

[26] Sébastien Michelin and Eric Lauga. Optimal feeding is optimal swimming for all Péclet numbers. *Phys. Fluids*, 23(10):101901, 2011.

[27] Julius B. Kirkegaard and Raymond E Goldstein. Filter-feeding, near-field flows, and the morphologies of colonial choanoflagellates. *Phys. Rev. E*, 94(5):052401, 2016.

[28] S. V. Patankar. *Numerical Heat Transfer and Fluid Flow*. Hemisphere, 1980.

[29] Thomas Kiørboe and Andrew G Hirst. Shifts in mass scaling of respiration, feeding, and growth rates across life-form transitions in marine pelagic organisms. *The American Naturalist*, 183(4):E118–E130, 2014.

[30] S. G. Gordon. *Animal Physiology: Principles and adaptations*. Macmillan Publishing Co, New York, 2nd edition, 1972.

[31] Julia Dölger, Lasse Tor Nielsen, Thomas Kiørboe, and Anders Andersen. Swimming and feeding of mixotrophic biflagellates. *Scientific Reports*, 7, 2017.

[32] H. C. Berg. *Random walks in biology*. Princeton University Press, 1993.

[33] Jeff Shimeta and M. A. R. Koehl. Mechanisms of particle selection by tentaculate suspension feeders during encounter, retention, and handling. *J. Exp. Mar. Biol. Ecol.*, 209(1-2):47–73, 1997.

[34] Mark Dayel and Nicole King. Prey capture and phagocytosis in the choanoflagellate *Salpingoeca rosetta*. *PLoS one*, 9(5):e95577, 2014.

[35] Mark Dayel, Rosanna Alegado, Stephen Fairclough, Tera Levin, Scott Nichols, Kent McDonald, and Nicole King. Cell differentiation and morphogenesis in the colony-forming choanoflagellate *Salpingoeca rosetta*. *Develop. Biol.*, 357(1):73–82, 2011.

[36] Arnau Sebé-Pedrós, Pawel Burkhardt, Núria Sánchez-Pons, Stephen R. Fairclough, B. Franz Lang, Nicole King, and Inaki Ruiz-Trillo. Insights into the origin of metazoan filopodia and microvilli. *Mol. Bio. Evol.*, 30(9):2013–2023, 2013.

[37] Tarja T. Hoffmeyer and Pawel Burkhardt. Choanoflagellate models-*Monosiga brevicollis* and *Salpingoeca rosetta*. *Curr. Opin. Struct. Biol.*, 39:42–47, 2016.

[38] Julius B. Kirkegaard, Alan O. Marron, and Raymond E. Goldstein. Motility of colonial choanoflagellates and the statistics of aggregate random walkers. *Phys. Rev. Lett.*, 116(3):038102, 2016.

[39] Marcus Roper, Mark J. Dayel, Rachel E. Pepper, and M. A. R. Koehl. Cooperatively generated stresslet flows supply fresh fluid to multicellular chanoflagellate colonies. *Phys. Rev. Lett.*, 110:228104, 2013.

[40] Michala E. Pettitt. *Prey capture and ingestion in choanoflagellates*. PhD thesis, University of Birmingham, 2001.

[41] Tom Fenchel. Suspended marine bacteria as a food source. In *Flows of energy and materials in marine ecosystems*, pages 301–315. Springer, 1984.

[42] Tom Fenchel. Protozoan filter feeding. *Prog. Protistol.*, 1:65–113, 1986.

[43] Barry S. C. Leadbeater. *The Choanoflagellates: Evolution, Biology and Ecology*. Cambridge University Press, Cambridge, 1 edition, 2015.

[44] Jasmine L. Mah, Karen K. Christensen-Dalsgaard, and Sally P. Leys. Choanoflagellate and choanocyte collar-flagellar systems and the assumption of homology. *Evol. & Develop.*, 16(1):25–37, 2014.

[45] Manuel Maldonado. Choanoflagellates, choanocytes, and animal multicellularity. *Invertebrate Biol.*, 123(1):1–22, 2004.

[46] Lasse Tor Nielsen, Sayed Saeed Asadzadeh, Julia Dölger, Jens H. Walther, Thomas Kiørboe, and Anders Andersen. Hydrodynamics of microbial filter feeding. *Proc. Natl. Acad. Sci. USA*, 114(35):9373–9378, 2017.

[47] E. M. Purcell. Life at low Reynolds number. *Am. J. Phys.*, 45(1):3–11, 1977.

[48] Eric Lauga and Thomas R. Powers. The hydrodynamics of swimming microorganisms. *Rep. Prog. Phys.*, 72(9):096601, 2009.

[49] Thomas Kiørboe. How zooplankton feed: mechanisms, traits and trade-offs. *Biol. Rev.*, 86(2):311–339, 2011.

[50] Ejnar Jules Fjerdingstad. The ultrastructure of choanocyte collars in *Spongilla lacustris* (l.). *Z. Zellforsch.*, 53(5):645–657, 1961.

[51] Dorte Mehl and H. M. Reiswig. The presence of flagellar vanes in choanomeres of Porifera and their possible phylogenetic implications. *J. Zoo. Sys. Evol. Res.*, 29(4):312–319, 1991.

[52] Norbert Weissenfels. The filtration apparatus for food collection in freshwater sponges (Porifera, Spongillidae). *Zoomorph.*, 112(1):51–55, 1992.

[53] Barry S. C. Leadbeater. The mystery of the flagellar vane in choanoflagellates. *Nova Hedwigia Beiheft*, 130:213, 2006.

[54] Sayed Saeed Asadzadeh, Poul S. Larsen, Hans Ulrik Riisgård, and Jens H. Walther. Hydrodynamics of the leucon sponge pump. *J. Roy. Soc. Inter*, (submitted), 2018.

[55] Poul Scheel Larsen and Hans Ulrik Riisgård. The sponge pump. *J. Theor. Biol.*, 168:53–63, 1994.

[56] S. P. Leys, G. Yahel, A. Reidenbach, V. Tunnicliffe, U. Shavit, and H. Reiswig. The sponge pump: the role of current induced flow in the design of the sponge body plan. *PLoS one*, 6(12):e27787, 2011.

[57] D. A. Ludeman, M. A. Reidenbach, and S. P. Leys. The energetic cost of filtration by demosponges and their behavioural response

to ambient currents. *J. Exp. Biol.*, 220(6):995–1007, 2017.
[58] Per Andersen. Functional biology of the choanoflagellate *Diaphanoeca grandis Ellis*. *Marine Microbial Food Webs*, 3(2):35–50, 1988.
[59] A. E. Walsby and Anastasia Xypolyta. The form resistance of chitan fibres attached to the cells of Thalassiosira fluviatilis Hustedt. *British Phycological Journal*, 12(3):215–223, 1977.
[60] Michala E. Pettitt, Belinda A. A. Orme, John R. Blake, and Barry S. C. Leadbeater. The hydrodynamics of filter feeding in choanoflagellates. *Eur. J. Protist.*, 38:313–332, 2002.
[61] J. J. L. Higdon. A hydrodynamic analysis of flagellar propulsion. *J. Fluid Mech.*, 90(4):685–711, 1979.
[62] M. A. Sleigh. Mechanisms of flagellar propulsion. *Protoplasma*, 164(1-3):45–53, 1991.
[63] G. K. Batchelor. *An Introduction To Fluid Dynamics*. Cambridge University Press, 1. edition, 1967.
[64] N. R. Silvester. Some hydrodynamic aspects of filter feeding with rectangular-mesh nets. *J. Theor. Biol.*, 103(2):265–286, 1983.
[65] John Happel and Howard Brenner. *Low Reynolds number hydrodynamics*. Kluwer Academic Publishers, 2 edition, 1983.
[66] Sébastien Michelin and Eric Lauga. Optimal feeding is optimal swimming for all Péclet numbers. *Phys. Fluids*, 23(10):101901, 2011.
[67] Julius B. Kirkegaard and Raymond E Goldstein. Filter-feeding, near-field flows, and the morphologies of colonial choanoflagellates. *Phys. Rev. E*, 94(5):052401, 2016.
[68] S. V. Patankar. *Numerical Heat Transfer and Fluid Flow*. Hemisphere, 1980.
[69] Thomas Kiørboe and Andrew G Hirst. Shifts in mass scaling of respiration, feeding, and growth rates across life-form transitions in marine pelagic organisms. *The American Naturalist*, 183(4):E118–E130, 2014.
[70] S. G. Gordon. *Animal Physiology: Principles and adaptations*. Macmillan Publishing Co, New York, 2nd edition, 1972.
[71] Julia Dölger, Lasse Tor Nielsen, Thomas Kiørboe, and Anders Andersen. Swimming and feeding of mixotrophic biflagellates. *Scientific Reports*, 7, 2017.
[72] H. C. Berg. *Random walks in biology*. Princeton University Press, 1993.
[73] Jeff Shimeta and M. A. R. Koehl. Mechanisms of particle selection by tentaculate suspension feeders during encounter, retention, and handling. *J. Exp. Mar. Biol. Ecol.*, 209(1-2):47–73, 1997.
[74] Mark Dayel and Nicole King. Prey capture and phagocytosis in the choanoflagellate *Salpingoeca rosetta*. *PLoS one*, 9(5):e95577, 2014.
[75] Mark Dayel, Rosanna Alegado, Stephen Fairclough, Tera Levin, Scott Nichols, Kent McDonald, and Nicole King. Cell differentiation and morphogenesis in the colony-forming choanoflagellate *Salpingoeca rosetta*. *Develop. Biol.*, 357(1):73–82, 2011.
[76] Arnau Sebé-Pedrós, Pawel Burkhardt, Núria Sánchez-Pons, Stephen R. Fairclough, B. Franz Lang, Nicole King, and Inaki Ruiz-Trillo. Insights into the origin of metazoan filopodia and microvilli. *Mol. Bio. Evol.*, 30(9):2013–2023, 2013.
[77] Tarja T. Hoffmeyer and Pawel Burkhardt. Choanoflagellate models-*Monosiga brevicollis* and *Salpingoeca rosetta*. *Curr. Opin. Struct. Biol.*, 39:42–47, 2016.
[78] Julius B. Kirkegaard, Alan O. Marron, and Raymond E. Goldstein. Motility of colonial choanoflagellates and the statistics of aggregate random walkers. *Phys. Rev. Lett.*, 116(3):038102, 2016.
[79] Marcus Roper, Mark J. Dayel, Rachel E. Pepper, and M. A. R. Koehl. Cooperatively generated stresslet flows supply fresh fluid to multicellular chanoflagellate colonies. *Phys. Rev. Lett.*, 110:228104, 2013.
[80] Michala E. Pettitt. *Prey capture and ingestion in choanoflagellates*. PhD thesis, University of Birmingham, 2001.

IX. SUPPLEMENTARY INFORMATION

Model morphology of Diaphanoeca grandis

To prepare the geometry of *D. grandis* for CFD simulations, we use data collated from six individuals that are viewed from the side [6]. We assume that the cell surface and the outline of the lorica have rotational symmetry about the longitudinal axis. In polar spherical coordinates, the cell and the outline of the lorica are described as:

$$R(\theta) = R_0(1 + \alpha_1 \cos\theta + \alpha_2 \cos 2\theta + \alpha_3 \cos 3\theta) \quad \text{(S1)}$$

where θ is the polar angle, and R_0, α_1, α_2 and α_3 are shape parameters. Table S1 describes the shape parameters used for the cell and the lorica dome. The centerline of a single microvillus with circular cross-section of radius $0.075\,\mu$m is described as:

$$R_F(\theta) = R_C(\theta_C) + [R_L(\theta_L) - R_C(\theta_C)]\frac{\theta - \theta_C}{\theta_L - \theta_C} \quad \text{(S2)}$$

where $\theta_L = 25$ deg and $\theta_C = 76$ deg are angles where the microvillus connects to the cell and the lorica, respectively. This microvillus is then copied in a circular pattern to obtain 50 evenly distributed microvilli to construct the collar filter.

case	R_0 (μm)	α_1	α_2	α_3
Cell	2.8	-0.24	0.10	-0.10
Lorica	8.1	0.15	0.05	0.00

TABLE S1: Average morphology parameters used to describe the cell and outline of the lorica

Movies

Movie S1 shows a video recording of freely swimming individual of *D. grandis*. Movies S2 and S3 show the CFD simulation of the freely swimming *D. grandis* with and without its lorica, respectively.